Multimodal High-Resolution Imaging in Retinitis Pigmentosa: A Comparison Between Optoretinography, Cone Density, and Visual Sensitivity

Benjamin J. Wendel,[1] Vimal Prabhu Pandiyan,[1] Teng Liu,[1] Xiaoyun Jiang,[1] Ayoub Lassoued,[1] Emily Slezak,[1] Sierra Schleufer,[1] Palash Bharadwaj,[1] William S. Tuten,[2] Debarshi Mustafi,[1,3] Jennifer R. Chao,[1] and Ramkumar Sabesan[1]

[1]Department of Ophthalmology, University of Washington School of Medicine, Seattle, Washington, United States
[2]Herbert Wertheim School of Optometry & Vision Science, University of California Berkeley, Berkeley, California, United States
[3]Seattle Children's Hospital, Seattle, Washington, United States

Correspondence: Ramkumar Sabesan, University of Washington School of Medicine, Department of Ophthalmology, 750 Republican St., E-213, UW Ophthalmology SLU campus, Seattle, WA 98109, USA; rsabesan@uw.edu.

Received: March 24, 2024
Accepted: August 2, 2024
Published: August 29, 2024

Citation: Wendel BJ, Pandiyan VP, Liu T, et al. Multimodal high-resolution imaging in retinitis pigmentosa: A comparison between optoretinography, cone density, and visual sensitivity. *Invest Ophthalmol Vis Sci.* 2024;65(10):45. https://doi.org/10.1167/iovs.65.10.45

Purpose. Retinitis pigmentosa (RP), the most common inherited retinal disease, is characterized by progressive photoreceptor degeneration. It remains unknown to what extent surviving photoreceptors transduce light and support vision in RP. To address this, we correlated structure and functional measures using adaptive optics scanning laser ophthalmoscopy (AOSLO), adaptive optics microperimetry, and adaptive optics optical coherence tomography (AO-OCT)–based optoretinograms (ORGs).

Methods. Four patients with RP were imaged with AOSLO across the visual field covering the transition zone (TZ) of normal to diseased retina. Cone density was estimated in discrete regions spanning the TZ. Visual sensitivity was assessed by measuring increment thresholds for a 3-arcmin stimulus targeted via active eye tracking in AOSLO. ORGs were measured at the same locations using AO-OCT to assess the cones' functional response to a 528 ± 20-nm stimulus. Individual cone outer segment (COS) lengths were measured from AO-OCT in each subject.

Results. Cone density was significantly reduced in patients with RP. Density reduction correlated with TZ location in 3 patients with RP, while a fourth had patches of reduced density throughout the retina. ORG amplitude was reduced in regions of normal and reduced cone density in all patients with RP. ORG response and COS length were positively correlated in controls but not in patients with RP. Despite deficits in cone density and ORG, visual sensitivity remained comparable to controls in three of four patients with RP.

Conclusions. ORG-based measures of retinal dysfunction may precede deficits in cone structure and visual sensitivity. ORG is a sensitive measure of RP disease status and has significant potential to provide insight into disease progression and treatment efficacy.

Keywords: optoretinography, adaptive optics, functional imaging, retinitis pigmentosa

Retinitis pigmentosa (RP) refers to a group of clinically similar phenotypes with genetically heterogeneous causes. The discovery of the first causative gene in 1990[1] and subsequent discovery of over 80 causative genes for RP[2] have provided further insight into the pathophysiology of disease. RP is broadly characterized by a gradual loss of rods resulting in night-vision impairment and progressive peripheral visual field loss followed by secondary cone degeneration, leading to severe visual impairment and central vision loss. The clinical diagnosis of RP currently relies on structural and functional measures of retinal integrity, including clinical ophthalmoscopy, optical coherence tomography (OCT), visual perimetry, and electroretinography (ERG). One of the central findings in RP is disruption to the reflective bands on OCT emanating from the photoreceptors. As visualized by OCT, the transition zone (TZ) is the region of active photoreceptor degradation that separates a "central island" of relatively healthy-appearing retina from the more severely diseased peripheral retina. While the principal biomarkers of RP in the clinic signal broader regional changes in the retina, we still lack a detailed understanding of disease status and photoreceptor function at a cellular level.

Adaptive optics (AO) has enabled probing the structural features at the cellular level in patients with RP and those afflicted with other retinal diseases.[3] AO-scanning laser ophthalmoscopy (AOSLO) images of patients with RP have shown a variety of structural phenotypes depending on disease severity, including normal-appearing cone mosaic in the central macula, cones with abnormal waveguiding in the TZ that appear dysflective (abnormal reflections),[4–6] and

severely disrupted mosaics that extend beyond the TZ. For the cone mosaic that remains intact, it has been established that cone density decreases and cell diameter increases in the TZ of patients with RP.[4] Moreover, even when cone density is reduced by up to 62% below normal controls near the fovea, visual acuity and sensitivity detected by current clinical measures remained within normal limits.[7] Thus, despite the advances in our ability to discern cone structure, there is a need to develop tools with the sensitivity and resolution to assess cone function as well at a cellular scale in RP.

Cellular-scale measures of cone dysfunction in RP have been limited in comparison to the AO-based structural metrics. AO-microperimetry (AOMP) corrects for eye movements in real time by actively tracking the retinal image, enabling the delivery of visual stimuli to specific cellular targets, thereby overcoming the limited spatial specificity of conventional microperimetry.[8] In RP, for example, the use of AOMP has shown that there is a decrease in visual sensitivity in patients with mutations in the RPGR gene but not in those with patients with RHO mutation. Clearly, the specific mutation in RP affects the mechanisms by which disease manifests in cone structure and function.[9]

While all perimetric techniques, including AOMP, depend on subjective feedback, the gold standard for objective functional assessment is ERG. Although a full-field ERG is a widely used functional test for the diagnosis of RP, its use is restrictive in monitoring disease progression because of the lack of spatial resolution. Even multifocal ERGs (mfERG) have relatively coarse spatial resolution compared to other functional assays such as macular visual field sensitivity and microperimetry.[10] ERGs measure the composite response of large numbers of cones (e.g., ∼1.5° of retina in mfERG) and are not measurable in advanced stages of disease. ERGs lack the sensitivity to identify local variation in retinal response, let alone probe retinal function at the level of individual cells. Moreover, ERG requires subject cooperation with electrode placement and can be challenging in the pediatric population.

Thus, there is a need for noninvasive retinal imaging that would provide cellular-scale resolution to assess the structural and functional state of the retina. Recent advances in the use of AO-OCT to generate optoretinograms (ORGs) have made it possible to quantify light-evoked responses in the retina in an objective manner and at the level of single cells with exquisite spatiotemporal resolution.[11–16] This can lead to a sensitive and comprehensive assay of cone viability in RP. The technology is still relatively nascent in its application to retinal diseases and has shown promising early results. Lassoued et al.[17] compared AO-OCT–derived measures of cone density, cone outer segment length (COS), and ORG as well as clinical measures of visual sensitivity. They reported ORG responses were reduced in RP, even in areas of apparently normal cone mosaics, indicating that ORGs can detect dysfunction that may remain undetectable with other measures. In another recent study, Gaffney et al.[18] reported subclinical deficits in RP using AOSLO-derived intensity-based ORGs. To what extent deficits observed in ORG are correlated with extant measures of cellular structure and function from AOSLO and AO retinally contingent microperimetry remains uncharacterized. For future applicability, it is not only important to compare findings across different instruments and variants of ORG but also against the more prevalent measures of high-resolution cone structure such as AOSLO. Our objective was to combine the cellular-scale imaging tools of AOSLO, AOMP, and ORG in the same individual patients with RP and to evaluate the degree of correlation and covariance in these biomarkers. Correlating the measures enables the assessment of the sensitivity of these different metrics to disease and addresses the inherent sources of limitations within each. We hypothesize that ORG is more sensitive to cellular dysfunction than AOMP and that it can be used to identify cells afflicted by disease where there are no apparent structural defects. In combination, these biomarkers that are all acquired via safe and noninvasive tools will enable creation of a severity score that can be used for assessing disease progression and the efficacy of new targeted therapies in the future.

Methods

Four patients (ages 25–30) clinically diagnosed with RP on the basis of ophthalmologic exams and family history at the Karalis Johnson Retina Center, Department of Ophthalmology at University of Washington were enrolled in the study. Research procedures followed the tenets of the Declaration of Helsinki. Age-similar normal controls were also enrolled in the study. Informed consent was obtained from all patients, and research protocols were approved by the institutional review board of the University of Washington (IRB#STUDY00002923).

Prior to experiments, a drop of 1% tropicamide was administered to dilate the pupil and arrest accommodation. RP patient biometrics are outlined in Table 1. The disease TZ was verified using clinical OCT (Spectralis HRA+OCT system; Heidelberg Engineering, Vista, CA, USA) according to previously described methods[19] and aligned to the AOSLO image montage as a reference for subsequent measurements of cone structure and function. Patients were then imaged with AOSLO across the four cardinal meridians of the visual field covering the TZ.

Individual AOSLO confocal reflectance images were stitched together to form a high-resolution retinal montage for each patient.[20] Regions of interest (ROIs) of size 100 × 100 µm were selected from the confocal image montage in locations where circular, unimodal reflections were packed in a roughly contiguous hexagonal mosaic. Because nonconfocal (also referred to as split detection or phase contrast) images were unavailable at the time of the study, we chose the ROIs starting from the first resolvable image near the fovea until the end of TZ, the point at which reflections from the inner-outer segment junction (ISOS) are absent on clinical OCT. Cones were identified using custom software and manually refined by two independent BJW graders. If there was more than 10% disparity between the two BJW graders, a third BJW grader was included for arbitration. The two closest values were then averaged. The same process was repeated for controls (n = 7). In one patient (RP039), an AOSLO follow-up was performed using split detection 32 months after the original study visit. Split detection procedures were conducted as in Scoles et al.[21]

Table 1. Biometrics of Patients Diagnosed With RP

Subject ID	Age	Sex	Genotype	TZ Start	TZ End
RP025	25	F	Indeterminate	1.3° inferior	3.0° inferior
RP039	28	M	IMPDH1	2.5° inferior	5.0° inferior
RP040	29	F	RHO	3.4° inferior	4.4° inferior
RP062	30	F	SNRNP200	2.6° temporal	4.5° temporal

Visual sensitivity was assessed in AOSLO by measuring increment thresholds to a 535 ± 7-nm stimulus presented for 500 ms against a 4.35-cd/m^2 background. AOMP stimuli were ~3 arcmin in diameter, approximately 74 times smaller than the Goldmann III stimulus used in standard perimetry. Stimuli were targeted to retinal locations using real-time eye tracking,[8] and their intensities were modulated using a yes/no adaptive staircase procedure guided by the QUEST algorithm.[22] Two interleaved staircases comprising 15 to 20 stimulus presentations converged to a sensitivity threshold, and repeat measurements were acquired when convergence was inadequate. In one test location where the stimulus was not seen due to the severity of the disease (RP025, 6°), sensitivity was assigned a value of 0 dB. Transverse chromatic aberration was measured between the imaging and stimulus channels for each experiment. The retinal locations chosen for microperimetry aligned with the site of cone density and ORG measurements.

ORGs were measured with line-field spectral domain AO-OCT to assess cone function.[42,43] The change in optical path length (ΔOPL) between the cone outer segment tips (COST) and ISOS reflections in AO-OCT following a bleaching stimulus provided a measure of light-evoked activity in the outer segment. ORGs were acquired with a 528 ± 20-nm light stimulus, corresponding to a nominal photon density of 1.5×10^7 photons/μm^2. Patients were dark adapted for 1 to 3 minutes, and OCT volumes were acquired for 2.5 seconds at a rate of 15 volumes/s over a field size of 1.0° × 1.3°. Each OCT recording comprised 40 volumes, which were repeated 5 to 10 times at each ROI for each subject. AO-OCT image processing followed conventional techniques and has been published previously.[11,42,43] Briefly, reconstructed AO-OCT volumes were segmented and registered to yield en face images of the COST and ISOS layers, from which individual cones were selected for the extraction of ORGs. For ORGs, the phase analysis followed Hillmann et al.[13] and yielded, as the final product, the temporal evolution of ΔOPL in individual cone outer segments in response to the stimulus.

COS length was evaluated by identifying the reflections corresponding to ISOS and COST at subpixel resolution using a three-dimensional center-of-mass algorithm in 5138 control and 3575 RP cones. The algorithm automatically identifies ISOS and COST peak reflections based on an assigned depth range. The automatic procedure was refined by manual graders for all RP (n = 3575) and a subset of control (n = 1554/5138) COS lengths. For the manual procedure, each cone's A-line reflectance profile was cross-referenced with the OCT en face image, and cones with ISOS or COST reflections that could not be verified were excluded from analysis (rejected cones, n = 5/1554 and 203/3575 for control and RP, respectively). Control COS lengths differed by less than 1% between automatic and manual methods. For seven of eight RP subject ROIs, mean COS lengths differed slightly (2.8%–11%) between methods, while RP040's 3-degree ROI differed by 24% due to poorer image quality. In general, the automatic method tended to overestimate COS length when compared to the manually verified method, likely due to confusion of the COST reflection with the retinal pigmented epithelial layer.

Then, the presence of a correlation was assessed between ΔOPL and individual COS lengths. Cones were clustered as either high or low ΔOPL for two-way ANOVA and linear regression comparisons. High and low ΔOPL thresholds were set to be 2 standard deviations from the mean of either the high- or low-response cluster in controls for each eccentricity. High/low ΔOPL thresholds were 348/172, 338/135, and 290/115 nm at 1°, 2°, and 3° eccentricity, respectively.

To determine whether cells with low ΔOPL were distributed randomly within an ROI, we employed Density Recovery Profile (DRP)[23] and Monte Carlo simulations as previously described to measure structure in S-cone submosaics.[24] The DRP measures the average density of a submosaic of interest as a function of distance from the points within that submosaic and plots the result as a histogram. Monte Carlo simulations are mosaics with the same overall cone positions as the submosaic population but randomly distributed within the mosaic. By comparing the measured DRP to the statistics of Monte Carlo DRPs, bin by bin in a histogram, it is possible to determine whether the measured distribution is significantly different from random. At close distances, a significantly low density of the DRP indicates that the cones in the submosaic are spaced apart, whereas a significantly high value indicates clumping. We generated 100 Monte Carlo simulated variants for every ROI to assess differences from a random arrangement. DRPs were computed with a bin width equal to the average nearest-neighbor distance of the local cone mosaic, such that the bins reflect the average density of cones approximately "x" number of cones away from one another. This enables capturing the degree of structure in the submosaic as it varies between individuals and eccentricity, unlike the case where bin widths are expressed in units of angular distance. A z-score ≥ 0.95 at any bin was used to gauge whether the measured DRP was significantly different from random.

Results

Retinal Structure in RP: OCT Outer Retinal Bands and High-Resolution AOSLO

The extent of disease progression was relatively similar across the four patients with RP, as assessed by the location of the TZ in conventional OCT. Mean TZ start was 2.47° ± 0.87°, and mean TZ length was 1.78° ± 0.64° (n = 4). For three of four patients, the TZ colocalized to cones with abnormal reflections (dysflective) in the AOSLO confocal image (Figs. 1B, 1C). In contrast, patient RP039's TZ aligned to a normal-appearing cone mosaic, whereas adjacent areas with intact photoreceptor bands on conventional SD-OCT scans showed abnormal cone structure in AOSLO (Fig. 1D).

Cone Density in AOSLO

Cone density was significantly reduced compared to controls in 21 of 41 ROIs across the four patients with RP ($P < 0.05$) (Fig. 2A). RP062 had normal densities compared to controls in the areas within and central to the TZ. RP025 had reduced density in all locations measured, including central to the TZ. RP040 had slightly reduced density, including central to the TZ. While density declined with increasing eccentricity in three of four patients (and controls), RP039 had dramatically reduced density near the fovea, yet normal or close to normal density at greater eccentricities, including in the TZ (see also Supplementary Fig. S5).

Retinal Function in RP: Visual Sensitivity With AO Microperimetry

Controls (n = 12) followed an expected eccentricity-dependent linear decline in sensitivity to 535-nm, 3

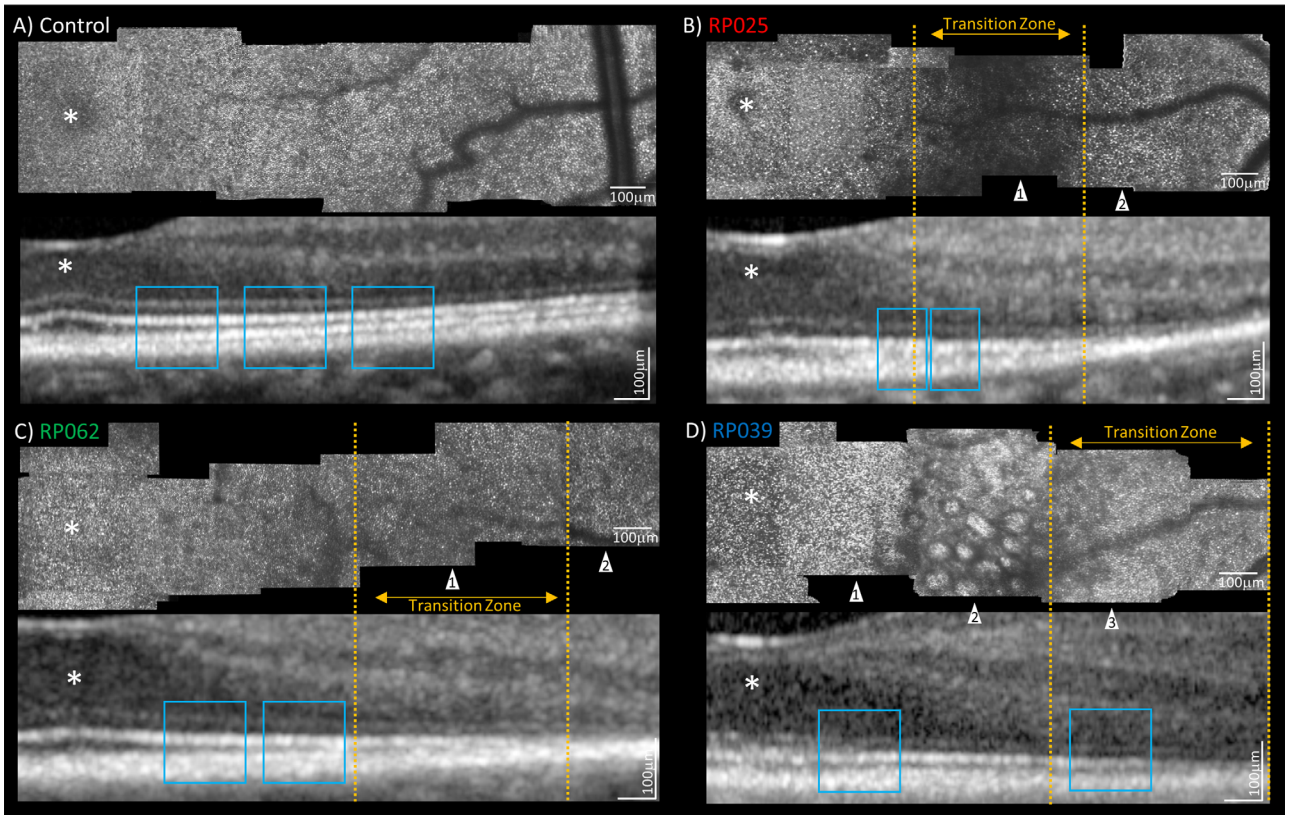

Figure 1. RP transition zone and ORG regions of interest. AOSLO montage (*top*) is aligned to OCT image (*bottom*) for each participant. *Stars* (*) mark the patients' fovea in AOSLO and OCT images (*top* and *bottom*, respectively). *Blue box* overlays on OCT B-scans represent the sites where ORG was measured. *Gold dashed lines* in patients with RP indicate the TZ. (**A**) Example from control subject AO001 showing normal cone mosaic in AOSLO and intact photoreceptor bands on OCT. In the RP subject (**B**, **C**), *arrows* 1 and 2 indicate regions of dysflective cones and retinal pigmented epithelial (RPE) cell mosaic, respectively. In the RP subject (**D**), *arrows* 1 and 2 indicate low cone density mosaic and abnormal reflections, respectively, both coaligned with intact photoreceptor bands on OCT. *Arrow* 3 indicates normal-appearing mosaic in the TZ, where reflections from the COST are absent in OCT.

arcmin retinally tracked increment stimuli (Fig. 2B). Each of the four patients with RP had locations with significantly reduced sensitivity, albeit with different patterns.

RP025 had normal sensitivity in areas of reduced cone density until the far end of the TZ. Thereafter, sensitivity reduced steadily until the stimulus was eventually not seen at all at 6°. The test site at 6° corresponded to a retinal location without reflections from the external limiting membrane (ELM) in OCT, consistent with results from a study using AOMP in macular telangiectasia type II where loss of sensitivity was correlated with lack of reflections in OCT from ELM but not the photoreceptor layers.[25]

Whereas RP025 retained normal levels of sensitivity prior to the TZ and even in areas of reduced density, RP062 had reduced sensitivity in all locations, including prior to the TZ and in areas of normal cone density. We observed a slight but significant decline in sensitivity at 1° (pre-TZ) and 6° (post-TZ) for RP039, with the remaining sites comparable in sensitivity to controls. RP040 sensitivity was normal near the fovea and at 1° but slightly reduced in the TZ. Although the four patients with RP were at relatively similar stages of disease progression with respect to TZ onset, there was no clear trend across patients on the degeneration's effect on visual sensitivity.

Retinal Function in RP: Single-Cone Optoretinograms

In normal controls, ORG responses to a 528-nm stimulus segregate into two clusters of ΔOPL, which is predicted by the differential cone spectral sensitivities to be LM-cones and S-cones, respectively. Example distributions of normal ORGs are shown in Supplementary Figure S1. We found RP ORGs to be degraded and variable to the extent that it was not possible to clearly distinguish between the expected two cone clusters as in controls. This poses the challenge of distinguishing cells with a diminished response from the expected population of cells, S-cones, that are minimally responsive to 528 nm light. To quantify ΔOPL degradation in RP, control ΔOPLs were first clustered into a low and high ΔOPL group at each eccentricity using Gaussian mixture model analysis. To quantify degradation of the ORG signal compared to controls, the mean of the high ΔOPL cluster minus two standard deviations was then set as the threshold for defining the high and low ΔOPL response subgroups in the patients with RP (see Methods).

A normalized cumulative histogram helped compare the distributions between controls and patients with RP. Two features are noteworthy for comparison. A shallower slope indicates greater variability (or variance of the distribution),

Investigative Ophthalmology & Visual Science

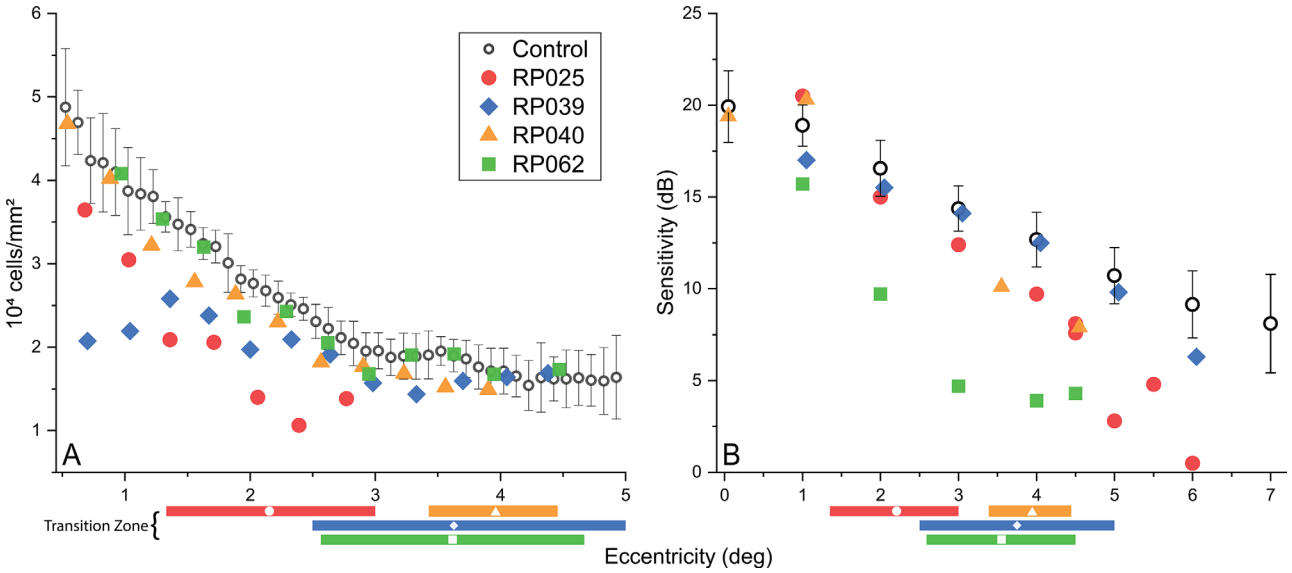

Figure 2. (**A**) Cone density in RP. Control values (*black open circles*) are a running average of 0.35° bins from seven controls. *Error bars* are the 95% confidence interval. Each RP data point is from a single confocal image. RP data points outside the control *error bars* are significantly different from controls ($P < 0.05$, 21/41 ROIs). Individual RP TZs are aligned to the x-axis in each patient's corresponding color and symbol. (**B**) Visual sensitivity in RP. Controls' ($n = 12$) mean sensitivity values and 95% confidence interval are shown in *black open circles*. As expected, sensitivity shows an eccentricity-dependent linear decline ($R^2 = 0.99$). Each RP data point is from an AOMP test for that patient. Individual RP TZs are aligned to the x-axis in each patient's corresponding color and symbol. The 0-dB result at 6° eccentricity in RP025 is offset from the axis for visibility.

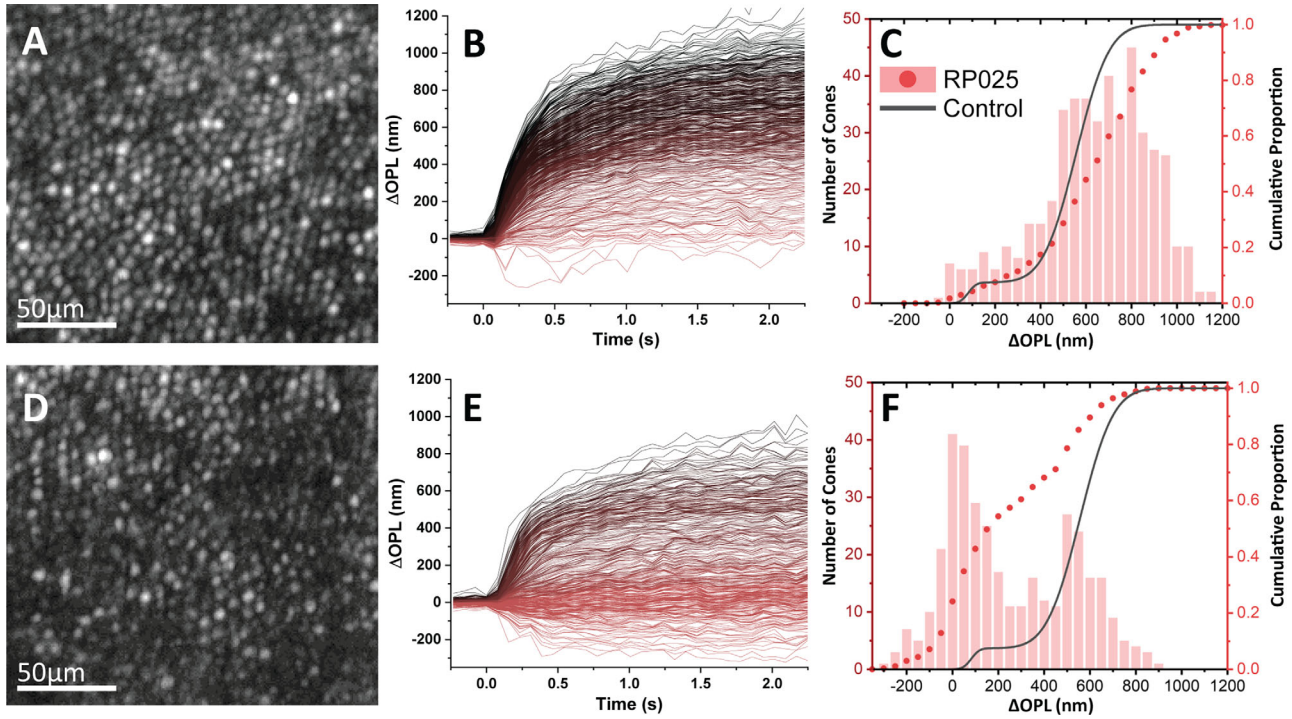

Figure 3. RP025 ORGs indicate degenerate cone response that increases with disease severity. (**A**, **D**) AO-OCT en face projection from the COST layer where ORG was obtained (1.7° inferior, *top*; 2.3° inferior, *bottom*). (**B**, **E**) Corresponding cone ORG responses for (**A**) and (**D**), respectively. Each *line* represents a single-cone ORG response. Histograms in (**C**) and (**F**) show the distribution of RP025 cone ORG responses (*red bars*; 50-nm bins) overlaid with RP025 (*red circles*) and mean control (*black line*) cumulative histograms.

and a leftward shift of the cumulative histogram curve on the x-axis indicates a lower average ΔOPL. For simplicity and comparison, we show the control subject ($n = 3$) mean fit overlain in the RP ORG in Figures 3 to 6.

In RP025, ORGs were acquired for two adjacent ROIs spanning the central TZ boundary and TZ (see Fig. 1, upper right panel). Both ORG sites overlap regions of significantly reduced density and normal visual sensitivity (red

Investigative Ophthalmology & Visual Science

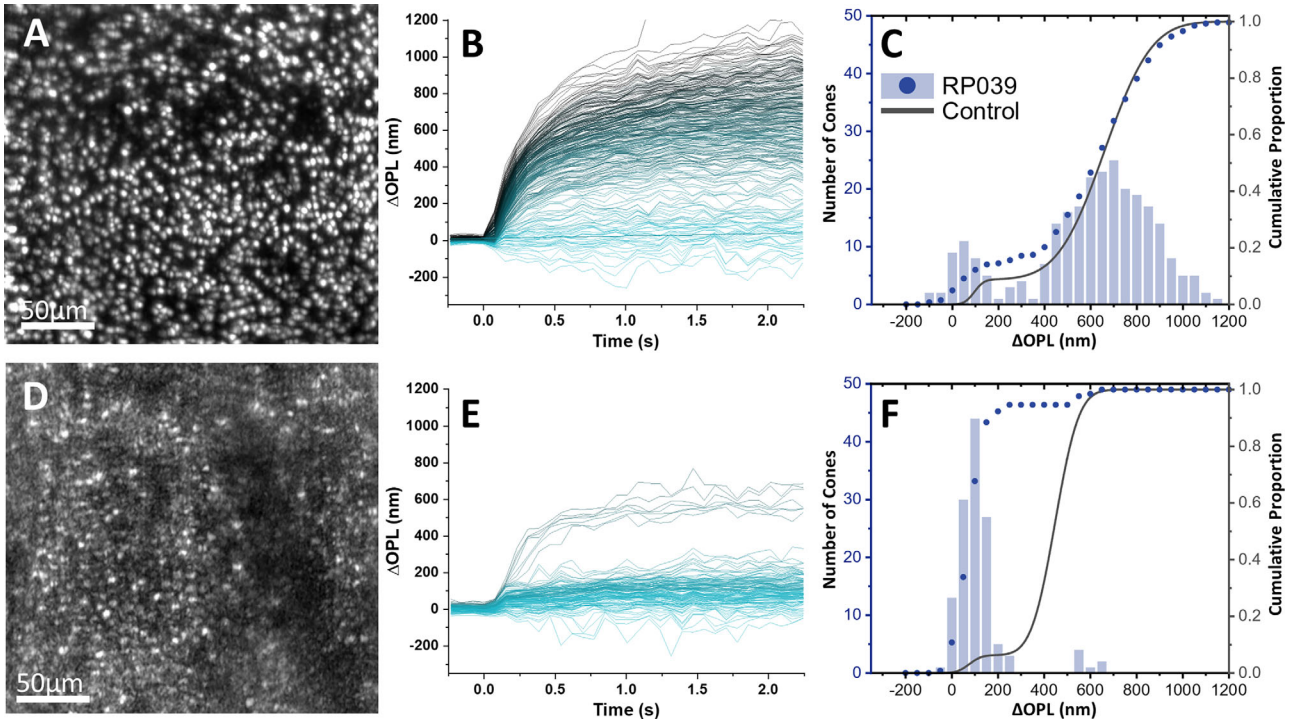

Figure 4. RP039 ORGs indicate cones with normal response in regions of predominantly degenerate cone responses. (**A**, **D**) AO-OCT en face projection from the COST layer where ORG was obtained (1° inferior, *top*; 3° inferior, *bottom*). (**B**, **E**) Corresponding cone ORG responses for (**A**) and (**D**), respectively. Each *line* represents a single-cone ORG response. Histograms in (**C**) and (**F**) show the distribution of RP039 cone ORG responses (*blue bars*; 50-nm bins) overlaid with RP039 (*blue circles*) and mean control (*black line*) cumulative histograms.

circles, Fig. 2). ORGs at 1.7° revealed nearly normal distribution of ΔOPL, yet with a slight but significant increase above controls in the number of cells with low ΔOPL (+5%, $P > 0.05$, Fig. 3). At TZ location 2.3°, ΔOPL is further degraded (+53%, $P > 0.005$). In both ORG sites, cells with a normal ΔOPL are intermingled with those that have a degraded response. Surprisingly, there is a small population (4.9%) of cells that showed a negative ΔOPL.

As shown in Figure 2A, RP039 was found to present an atypical structural phenotype: dramatically reduced density near the fovea, yet normal cone density in four of six ROIs measured in the TZ. ORGs at 1° revealed a slight but significant increase in the number of cells with low ΔOPL (+7.5%, $P < 0.05$) in a location with reduced density and slightly reduced sensitivity (Fig. 2, blue diamonds). However, at 3° eccentricity, ΔOPL is dramatically reduced (+88.7%, $P < 0.0005$), while density is slightly reduced, and visual sensitivity is comparable to controls. Strikingly, ~11% of the cones retained a normal ΔOPL, even in the context of an overall severely reduced ORG (Fig. 4).

RP040 ORGs were similar to normal controls at 1°, as were cone density and visual sensitivity (Fig. 2, yellow triangles). However, in the TZ at 3°, cone density was normal, and sensitivity was slightly reduced, while the ORG response was greatly reduced (+86.7% low ΔOPL cells, $P < 0.005$, Fig. 5). Negative ΔOPLs were also observed in the TZ of RP040.

In RP062, we observed increases in the number of low ΔOPL cells at both 1° (+29.3%, $P < 0.005$) and 2° (+21.6%, $P < 0.005$). In normal controls, the 528-nm stimulus segregates the cones into two discrete clusters of ΔOPL response, corresponding to L/M- and S-cones. In RP062, however, the histograms reveal three distinct clusters of ΔOPL (Fig. 6), in contrast to the graded distribution of reduced responses observed in the patients with RP above. The ORGs in RP062 corresponded to locations of normal (1°) and slightly reduced (2°) cone density but significantly reduced visual sensitivity (Fig. 2).

ORG Results Summary

Mean saturated ΔOPL was reduced in all four patients with RP compared to controls, and there was a higher proportion of cones with reduced ΔOPL at increasing eccentricity (Fig. 7A, $P < 0.05$). ΔOPL was likewise more variable in RP, as evidenced by the significantly greater standard deviation in Figure 7A and shallower slope in the cumulative histograms (Figs. 3–6). Seven of eight ROIs across the four patients had a significant increase in the number of cells with low ΔOPL compared to controls ($P < 0.05$, Fig. 7B), driving the increased variability in mean ΔOPL reported in Figure 7A. ROIs central to TZ had fewer low ΔOPL cells than those in the TZ in three of four patients with RP, while RP062 ORGs were similarly reduced in both ROIs central to the TZ (Fig. 7B). We observed cells with normal ΔOPLs in areas with otherwise moderate (RP025 and RP062) and severe (RP039) deficits in ORG (Figs. 3–5).

Cone Outer Segment Length and Correlation With ΔOPL Response

Given that photoreceptor outer segment lengths are known to shorten as the disease progresses in RP,[26] we sought to test whether a reduction in ΔOPL is correlated with COS length.

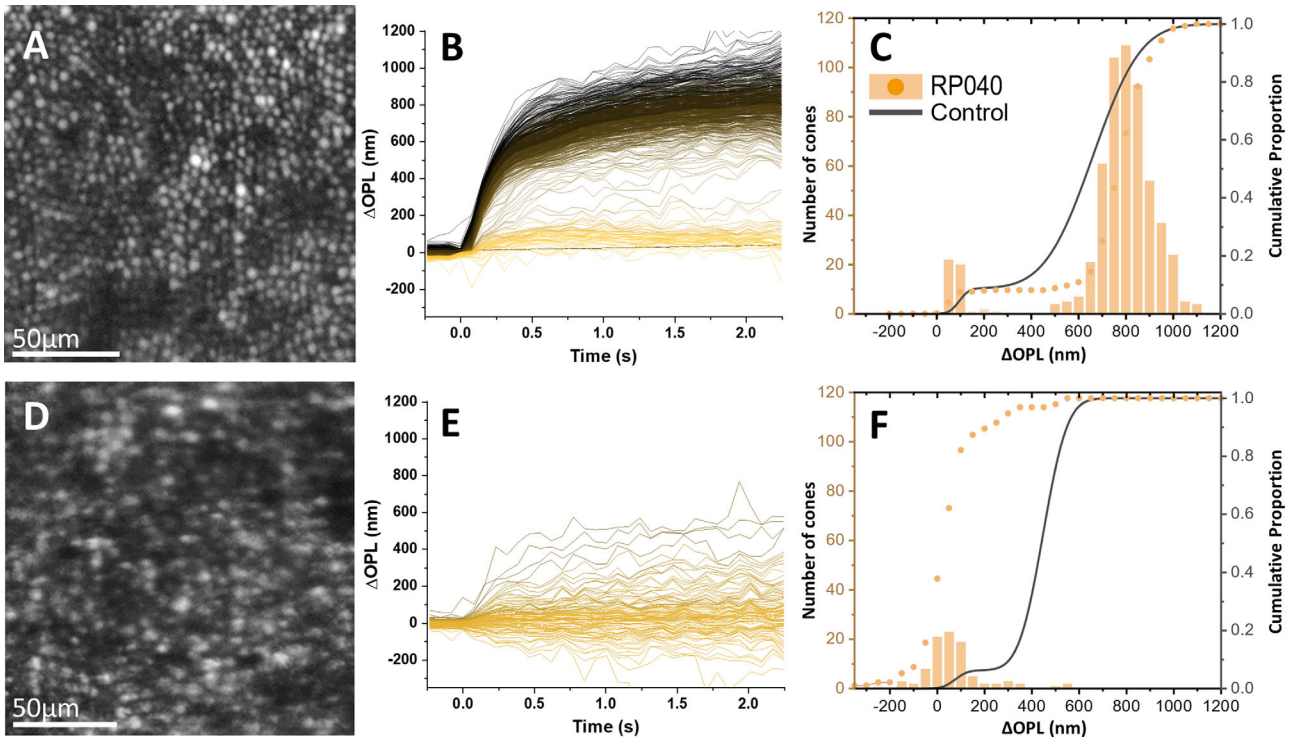

Figure 5. RP040 ORGs indicate cones with normal responses in the healthy zone and degenerate response in TZ. (**A**, **D**) AO-OCT en face projection from the COST layer where ORG was obtained (1° inferior, *top*; 3° inferior, *bottom*). (**B**, **E**) Corresponding cone ORG responses for (**A**) and (**D**), respectively. Each *line* represents a single-cone ORG response. Histograms in (**C**) and (**F**) show the distribution of RP040 cone ORG responses (*maize bars*; 50-nm bins) overlaid with RP039 (*maize circles*) and mean control (*black line*) cumulative histograms.

We tested 5138 control and 3323 RP cones for which ORGs were obtained. Control COS lengths were 34.2 ± 3.1 µm, 29.3 ± 2.7 µm, and 26.4 ± 2.6 µm for 1°, 2°, and 3° eccentricity. On average across eccentricity, low ΔOPL cones had 11.2% ± 3.6% shorter COS lengths than high ΔOPL cones in controls, purported to be S-cones.[27] While the range of RP COS lengths overlapped with controls (Supplementary Fig. S3), they were significantly more variable (n = 8/8 ROIs; t-test, $P < 0.05$) and shorter (n = 7/8 ROIs; one-way ANOVA, Games–Howell test, $P < 0.0005$). COS length was significantly longer than controls in one normal-appearing ROI in RP062 at 1° eccentricity. Within individual ROIs, COS length and ΔOPL in the high ΔOPL group were significantly correlated in controls and in three of four normal-appearing RP ROIs (R^2 = 0.02–0.15, $P < 0.05$) but not in the TZ of RP where ΔOPL was reduced (n = 4/4, $P > 0.05$, Supplementary Table S1). Two-way ANOVA and Fisher–Hayter contrasts between controls and RP revealed a significant interaction between outer segment (OS) lengths in high and low ΔOPL subgroups, driven by the fact that controls had a larger difference between the two subgroups than patients with RP (Supplementary Fig. S4). When combined across patients and eccentricities, ΔOPL scaled linearly with COS length in controls (R^2 = 0.26, $P < 0.05$), whereas the relationship broke down in the RP data (Fig. 8), most likely due to the drastic increase in variability in both ΔOPL and COS length.

Spatial Analysis of Low ΔOPL Cones

To assess whether cones with degraded ORGs are arranged randomly in the mosaic or tend to neighbor one another, we calculated DRP statistics (see Methods) on low ΔOPL cones in each RP mosaic. In RP025, RP039, and RP040, the spatial distribution of low ΔOPL cones was not significantly different from random as assessed by comparing their DRP to Monte Carlo simulations, suggesting that low ΔOPL cones did not tend to cluster in the mosaic. However, ROIs at 1° and 2° in RP062 were significantly different ($P < 0.05$) from random, indicating a higher likelihood for cells with degraded ORG to be clumped within one or two cones of each other at 1° and within a one-cone radius at 2° (Fig. 9). In comparison, normal controls exhibited a semi-regular arrangement of the low ΔOPL cones (i.e., S-cones), where they were unlikely to be situated within a radius twice the average distance between cones in that mosaic.

Discussion

The high-resolution, multimodal assessment of retinal structure and function in RP provides a sensitive and complementary view of the disease process. Overall, our data suggest that cone dysfunction in RP as measured by ORG can precede loss of visual sensitivity, as well as reduction in cone density and COS length. That this is a cross-sectional study in a small subset of patients, as opposed to a larger cohort longitudinal study, precludes a stronger conclusion on the timing of deterioration of these high-resolution structure and function phenotypes in RP. Below, we review the key high-resolution structure–function metrics in RP obtained from this study in the context of prior literature. We show the importance of comparing the ORG with more established measures of disease in the same patients with

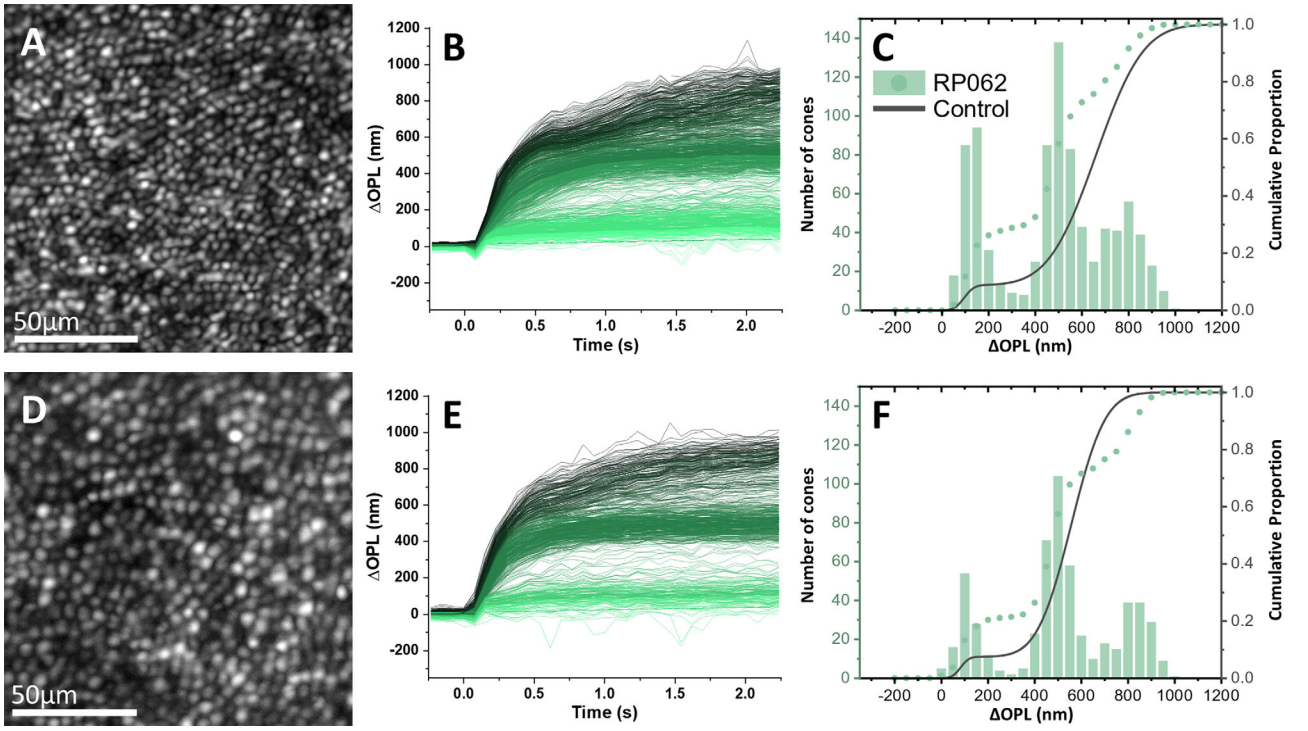

Figure 6. RP062 ORGs indicate cones with degenerate responses. (**A**, **D**) AO-OCT en face projection from the COST layer where ORG was obtained (1° temporal, *top*; 2° temporal, *bottom*). (**B**, **E**) Corresponding cone ORG responses for (**A**) and (**D**), respectively. Each *line* represents a single-cone ORG response. Histograms in (**C**) and (**F**) show the distribution of RP062 cone ORG responses (*green bars*; 50-nm bins) overlaid with RP062 (*green circles*) and mean control (*black line*) cumulative histograms.

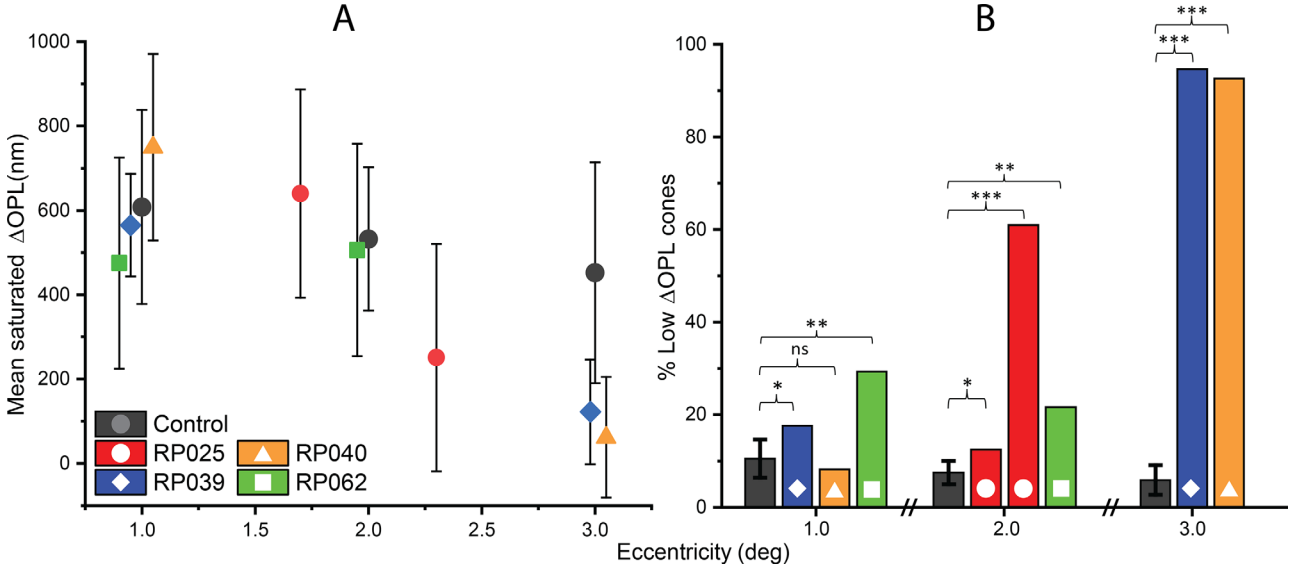

Figure 7. ORGs are reduced and more variable in RP. (**A**) Mean saturated ΔOPL comparison between control mean (*dark gray circles*, $n = 3$) ± 95% CI and individual RP ROIs. RP data points are offset from control for visibility. (**B**) Percentage of cones with low ΔOPL compared between controls (*gray bars*, ±1 SD, $n = 3$ patients) and RP ROIs at each eccentricity. *Asterisks* indicate a significant difference from controls: $^{*}P < 0.05$, $^{**}P < 0.005$, $^{***}P < 0.0005$.

RP—COS length, AOSLO cone density, and AOSLO-based microperimetry. Broadly, in the four RP cases presented here, we do not find a clear trend between deficits in visual sensitivity and high-resolution structural measures of cone density from AOSLO and individual COS lengths in AO-OCT. Of these, correlations between single COS length and ORG have been reported once before,[17] but our results were not entirely consistent with this prior report in normal controls, and we elaborate on the potential reasons for this discrepancy. ORGs were found to be a sensitive measure of

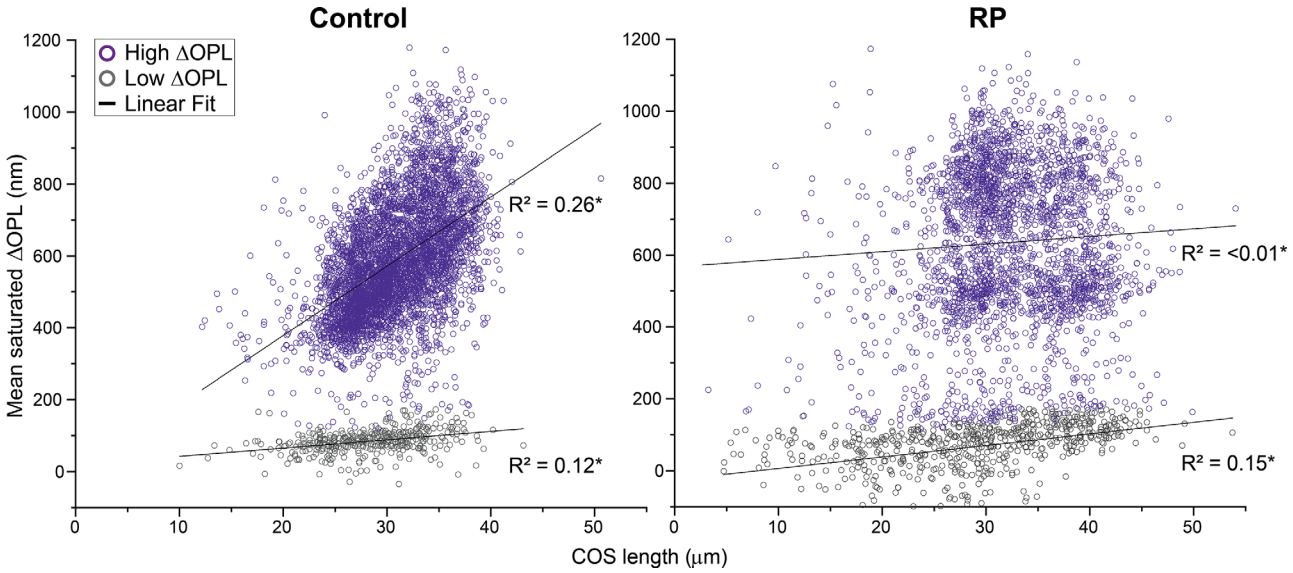

Figure 8. ΔOPL scales linearly with COS length in controls but not in RP. COS lengths are grouped by high (*purple*) and low (*gray*) ΔOPL subgroups in control and patients with RP for all ROIs tested (1°–3° eccentricity). For high and low ΔOPL subgroups, R^2 correlation coefficients are 0.26 and 0.12 for controls and <0.01 and 0.15 for RP, respectively. *Asterisk* indicates a significant correlation (ANOVA; $P < 0.05$). While the low ΔOPL versus COS length subgroups are statistically significant in both controls and RP, the R^2 values suggest only a weak linear correlation.

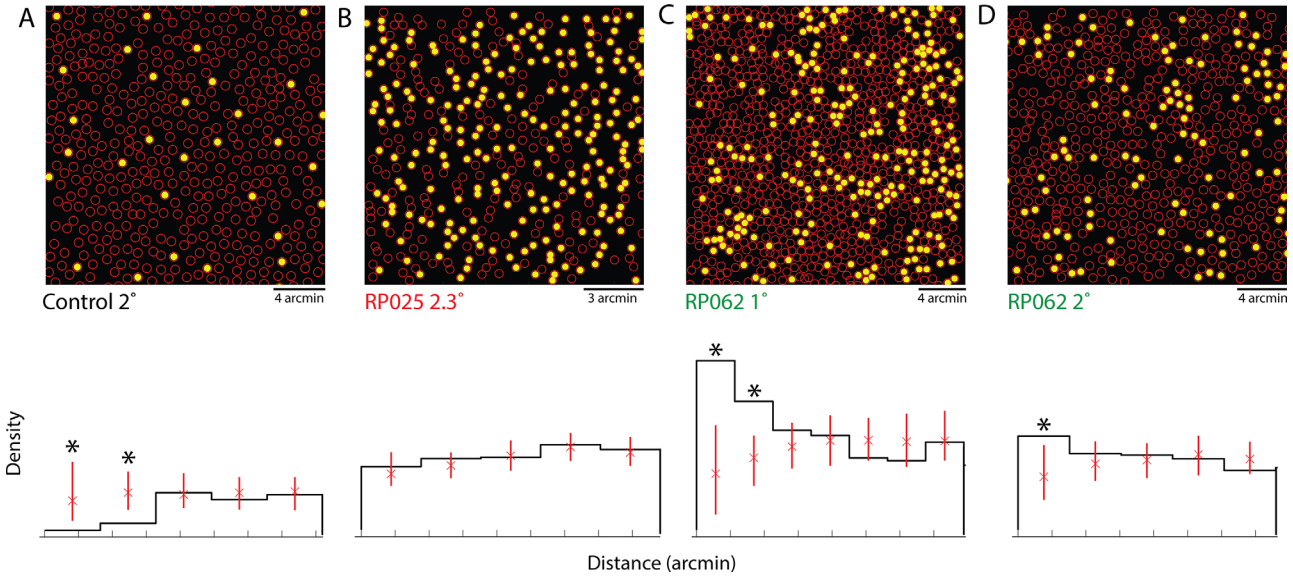

Figure 9. Cones with reduced ΔOPL show spatial clustering in RP062. *Top row*: RP cone mosaics showing spatial distribution of low ΔOPL cones (*yellow*). *Left to right*, low ΔOPL cells $n = 31/435$, <338 nm; $n = 222/400$, <338 nm; $n = 255/930$, <348 nm; $n = 122/589$, <338 nm. *Bottom row*: histogram for each mosaic compared to 100 randomly shuffled Monte Carlo simulations (*error bars* = 95% confidence interval) to test whether low ΔOPL cells are distributed randomly in the mosaic. Bin widths are set as the average intercone spacing for all cones in each mosaic (for A = 1.8, B = 1.8, C = 1.2, and D = 1.6 arcmin). *Asterisk* indicates bins that are either significantly lower (**A**) or higher (**C**, **D**) than the 95% confidence interval of the randomly shuffled mosaic. Results of the simulation indicate that low ΔOPL cells in RP062, shown in panels (**C**) and (**D**), exhibit significant clustering, but those of RP025 are not distinguishable from random (**B**). The low ΔOPL cones, i.e., S-cones, in controls (**A**) are arranged in a semi-crystalline manner (i.e., significantly spaced apart from each other than would be expected from a random distribution).

cone dysfunction, as reduced responses were observed in all patients with RP. While reductions in metrics of structure and function besides ORG are noted in most patients with RP, the consistency with which the disease manifests as a reduction in ORG is overall greater in comparison to other phenotypes at the same eccentricity. This is evident in Table 2, showing eccentricities where visual sensitivity and cone density are comparable to controls, but ORG is compromised. Even in ROIs with normal cone density ($n = 2/8$) and normal visual sensitivity ($n = 3/8$), ORGs were reduced significantly compared to controls. The converse scenario was never observed.

Investigative Ophthalmology & Visual Science

Table 2. Results Comparison of Different Metrics in Patients With RP Compared to Controls

RP Subject	RP025	RP039	RP040	RP062
ROI	**1.7° inferior**	**1° inferior**	**1° inferior**	**1° temporal**
Cone density	Reduced*	Reduced*	Normal	Normal
Visual sensitivity	Normal	Reduced*	Normal	Reduced*
ORG	Low ΔOPL*	Low ΔOPL*	Normal	Low ΔOPL**
COS length	Reduced*	Reduced*	Reduced*	Greater*
DRP spacing	Random	Random	Random	Clumped*
ROI	**2.3° inferior**	**3° inferior**	**3° inferior**	**2° temporal**
Cone density	Reduced*	Reduced*	Normal	Reduced*
Visual sensitivity	Normal	Normal	Reduced*	Reduced*
ORG	Low ΔOPL**	Low ΔOPL***	Low ΔOPL***	Low ΔOPL**
COS length	Reduced*	Reduced*	Reduced*	Reduced*
DRP spacing	Random	Random	Random	Clumped*

Asterisk indicates a significant difference from controls: *$P < 0.05$, **$P < 0.005$, ***$P < 0.0005$.

We observe no correlation between a decrease in visual sensitivity and either TZ onset or cone density. We find normal sensitivities in areas with reduced density (e.g., RP025), and TZ onset does not predict a drop in sensitivity (Fig. 2B). However, we also find instances of the opposite scenario, that is, deficits in visual sensitivity occurring in retinal regions with normal density (e.g., RP062 1° and 4° eccentricity), indicating that factors other than cone density and COS length may drive the deficit. While COSs are generally shorter in patients with RP, we do not find COS length derived from AO-OCT to be predictive of deficits in visual sensitivity (Table 2). Foote et al.[9] observed that cone spacing *z*-scores were correlated with OS thickness in patients with inherited retinal degenerations. Despite the variability of sensitivity measures in patients, OS thickness has been found to be a good predictor of retinal sensitivity.[28,29] However, this relationship seems to break down when correlating OS thickness to fundus-guided perimetry in a genetically heterogeneous group of patients with RP.[30] Our results are consistent with the latter, and the lack of a relationship between sensitivity and cone density is further attributed to a small patient cohort in our study. An added limitation here is the use of confocal as opposed to split-detection (also referred to as phase-contrast) images to estimate cone structure metrics, whereby cone density may be underestimated. This is most evident in RP039, where at the fovea and 1° eccentricity, a confocal image with a sparse cone mosaic with *empty* spaces is observed, but visual sensitivity is normal. The presence of non-waveguiding, albeit functional COS underlying intact inner segments may be a parsimonious explanation for this apparently normal visual sensitivity observed in RP039 at closer eccentricities. Although the split-detection mode of imaging was not available at the time of the study, the patient was imaged 32 months later with split detection, showing intact inner segments in areas corresponding to empty non-waveguiding cones in the confocal image (Supplementary Fig. S5). In macular telangiectasia,[25] loss of visual sensitivity measured with AOMP was similarly correlated with the loss of reflectance from the external limiting membrane in OCT but not with the loss of waveguiding cones in confocal AOSLO.

Consistent with the findings in Lassoued et al.,[17] in areas where cone density is reduced, we consistently see reductions in ORG, and that trend continues at increasing distances from the fovea into areas of more advanced disease. The ΔOPL is more variable in RP than in controls, and we find cells with a normal ORG response in the presence of cells with a degraded response. Surprisingly, in the three locations where we find greater than 50% reductions in ΔOPL, visual sensitivity remains normal. To what degree the two—ORG and visual sensitivity—are correlated mechanistically is a topic of future research. In comparing ORG and visual sensitivity, it is important to note that the ORG is measured at much higher stimulus light levels. On the other hand, while still in the photopic regime, the AOMP stimulus is a few orders of magnitude dimmer, although sufficient to evoke a visual percept representative of the sensitivity of the visual pathways underlying cones. The ORG response is suggestive of the functional capacity of the cones vis-à-vis bleaching, regeneration, and the phototransduction amplification cascade.

There are other reasons for the resilience *and* loss of visual sensitivity with retinal degenerations besides those based on structural phenotypes observed in the outer retina via OCT and AOSLO. For instance, it has been shown that patients with loss of up to ∼62% of cones still exhibit normal visual acuity and sensitivity.[7] Mechanisms of light adaptation in cones and downstream circuits can maintain visual sensitivity over a large range of light levels.[31] Thus, it can be expected that the same mechanisms can compensate for either reductions in photoisomerization rates caused by abnormal cone waveguiding or defects in the phototransduction cascade caused by specific genetic defects in RP. In the extreme case, in murine models of retinal degeneration, it has been shown that cone pathways remain sensitive to light even in cases of partial cone death[32] and when outer segments are lost to degeneration.[33] On the other hand, increased spontaneous neural activity originating in the inner retina in advanced RP contributes noise and reduces visual sensitivity.[34] For these reasons, objective assays of structure and function, such as the ORG, that are spatially localized to the photoreceptors have advantages over subjective measures of visual sensitivity for charting the course of disease progression.[35]

ORG deficits in RP are not correlated with COS length when taken as a whole, comparable to the findings of Lassoued et al.,[17] who concluded that cone OS length was a coarse predictor of ΔOPL. We find a weak correlation in the high ΔOPL groups in three of four patients with RP, when assessed within an ROI and eccentricity, in comparison to the higher correlations found previously. In controls, ΔOPL scaled linearly with COS length in the high ΔOPL group (∼19 nm ΔOPL/μm COS length for the stated bleaching level, Fig. 8A), unlike Lassoued et al.,[17] in which no corre-

Investigative Ophthalmology & Visual Science

lation was observed in controls. This inconsistency in correlations between studies is likely attributed to methodologic differences. Their metric of response strength combined the amplitude for three different wavelength stimuli using principal component analysis. The variation in response strength with cone OS length was then studied separately for each measured eccentricity and ROI. Here, the saturated ΔOPL was used as a measure of ORG response for a single-wavelength stimulus. Also, data were accumulated from different eccentricities to assay the variation of ΔOPL with cone OS length and mirrored the linear correlation seen across a larger eccentricity range in normal controls from 0° to 5°.[36] Supplementary Table S1 lists the cone OS length, ΔOPL, and their correlation for each ROI and eccentricity. The table demonstrates that the correlation in controls breaks down when analyzed separately for each ROI, similar to Lassoued et al.,[17] owing to the relative uniformity in outer segment length at a given eccentricity.

The linear relationship between ΔOPL and COS length is expected in controls under the hypothesis that the change in COS length is linked to water movement driven by an osmotic pressure imbalance caused by the amplified byproducts of phototransduction.[16,37] The saturated COS elongation, when interpreted as the OS reaching osmotic equilibrium, lets one apply Van't Hoff's law, where change in osmotic pressure is related to changes in the volume or length of the outer segment (assuming the width of the cone does not change). Given that cone outer segments exhibit an eccentricity-dependent variation in their length, the longer foveal COSs are posited to exhibit a larger saturated change in length (ΔOPL) than peripheral COS.

One limitation of measuring the cone ORG in RP (or any photoreceptor degenerative disease) is that the disease transition zone is defined clinically by a loss of outer retinal reflections, but the same reflections are required for measuring the cone ORG. Advanced methods may be used to locate remnant cone structure in the RP transition zone.[38] If deficits in ΔOPL in RP were explained by COS length alone, a 400-nm reduction in ΔOPL would require a 20-µm (or 58%–77%) reduction in COS length; such a reduction was not observed (Fig. 8B, Supplementary Table S1). While the greater variability in ΔOPL in RP was unexplained by COS length, it could be partially accounted for by abnormal waveguiding leading to intercone variability in photoisomerization. It is well documented that cone waveguiding is variable in retinal degenerations,[4–6] resulting in cones appearing dysflective in the confocal image and potentially less effective in channeling light into the photoreceptor outer segment. Although direct cellular measurements of waveguide efficiency and its effects on photoreceptor function in disease are lacking in RP, results from a psychophysical study have shown that patients with RP have reduced directional sensitivity compared to controls, which is attributed to changes in the alignment of macular cones.[39] The magnitude and rate of ΔOPL versus time are highly sensitive to bleach strength due to its large dynamic range[16]; small misalignments in the cone waveguide can decrease light capture and cause the ORG response to decrease and become more variable across cones. However, the amplification stages of phototransduction and mechanisms of light adaptation in cones can potentially rescue such changes in photoisomerization rates to maintain visual sensitivity. In such instances, high-resolution cone structure and visual sensitivity will both likely be less sensitive to disease progression, especially early in the disease process, when the OS is affected and the inner segment (IS) and the nuclei are remnant. Thus, ORG has significant potential to be a measure of individual cone waveguiding and structural viability.

RP062 (SNRNP200) presents a distinct phenotype compared to the other patients with RP. The ORG responses for RP062 were distributed in three discrete clusters of ΔOPL, and cones with a reduced response were more likely than random to be spatially adjacent. However, deficits in visual sensitivity were found in retinal regions with normal and slightly reduced cone density at 1° and 2° eccentricity, respectively. SNRNP200 mutations belong to a class of nonsyndromic autosomal dominant RP cases that are caused by ubiquitously expressed splice factors, which only affect the retina.[40] It remains unknown why SNRNP200 pathogenicity is specific to the retina, but it has been proposed that the mutation could cause either an accumulation of transcript errors that are toxic to the retina, defects in pre-mRNA splicing caused by high retinal metabolic demands, and/or SNRNP200 may serve additional functions in the retina that have yet to be described.[41] In the case of RP062, it is possible that the spatial clustering of discrete populations of dysfunctional cones could be driven by factors in the microenvironment that predispose sensitivity to the mutation, such as susceptibility to splicing errors and/or metabolic stress.

Overall, the changes in cone structure, as assessed via cone density and OS length, and changes in cone function, as assessed via microperimetry, are broadly consistent with published phenotypes in RP. The addition of ORG provides a highly sensitive assay of cone function and disease phenotypes, given how deficits are observed in seemingly normal areas of OCT and AOSLO. In addition, the ability to recognize a small fraction of healthy cells via ORG, in the presence of a largely diseased cell population, is important to identify targets and track their progression specific to the testing of future therapies. The multimodal evaluation of patients with RP has great promise for determining the pattern of disease progression at a photoreceptor level in specific RP genetic variants, as well as to establish outcome measures for ongoing and potential therapeutics.

Acknowledgments

The authors thank Jazlin Taylor and Alejandro Striefel for their contributions.

Supported by National Institutes of Health grants U01EY032055, EY029710, K08EY033789, P30EY001730; Research to Prevent Blindness Career Development Award; Burroughs Wellcome Fund Careers at the Scientific Interfaces; Foundation for Fighting Blindness; unrestricted grant from the Research to Prevent Blindness; Alcon Research Institute; Hellman Fellows Program; and George and Martina Kren Professorship in Vision Research; Dawn's Light Foundation.

Disclosure: **B.J. Wendel**, None; **V.P. Pandiyan**, (P); **T. Liu**, None; **X. Jiang**, None; **A. Lassoued**, None; **E. Slezak**, None; **S. Schleufer**, None; **P. Bharadwaj**, None; **W.S. Tuten**, (P); **D. Mustafi**, None; **J.R. Chao**, None; **R. Sabesan**, (P)

References

1. Dryja TP, McGee TL, Reichel E, et al. A point mutation of the rhodopsin gene in one form of retinitis pigmentosa. *Nature*. 1990;343:364–366.

2. Verbakel SK, van Huet RA, Boon CJ, et al. Non-syndromic retinitis pigmentosa. *Prog Retin Eye Res*. 2018;66:157–186.
3. Wynne N, Carroll J, Duncan JL. Promises and pitfalls of evaluating photoreceptor-based retinal disease with adaptive optics scanning light ophthalmoscopy (AOSLO). *Prog Retin Eye Res*. 2021;83:100920.
4. Sun LW, Johnson RD, Langlo CS, et al. Assessing photoreceptor structure in retinitis pigmentosa and Usher syndrome. *Invest Ophthalmol Vis Sci*. 2016;57:2428–2442.
5. Makiyama Y, Ooto S, Hangai M, et al. Macular cone abnormalities in retinitis pigmentosa with preserved central vision using adaptive optics scanning laser ophthalmoscopy. *PloS One*. 2013;8:e79447.
6. Duncan JL, Roorda A. Dysflective cones. *Adv Exp Med Biol*. 2019;1185:133–137.
7. Ratnam K, Carroll J, Porco TC, Duncan JL, Roorda A. Relationship between foveal cone structure and clinical measures of visual function in patients with inherited retinal degenerations. *Invest Ophthalmol Vis Sci*. 2013;54:5836–5847.
8. Tuten WS, Tiruveedhula P, Roorda A. Adaptive optics scanning laser ophthalmoscope-based microperimetry. *Optom Vis Sci*. 2012;89:563.
9. Foote KG, Wong JJ, Boehm AE, et al. Comparing cone structure and function in RHO- and RPGR-associated retinitis pigmentosa. *Invest Ophthalmol Vis Sci*. 2020;61:42–42.
10. Menghini M, Cehajic-Kapetanovic J, MacLaren RE. Monitoring progression of retinitis pigmentosa: current recommendations and recent advances. *Exp Opin Orphan Drugs*. 2020;8:67–78.
11. Pandiyan VP, Maloney-Bertelli A, Kuchenbecker JA, et al. The optoretinogram reveals the primary steps of phototransduction in the living human eye. *Sci Adv*. 2020;6:eabc1124.
12. Zhang F, Kurokawa K, Lassoued A, Crowell JA, Miller DT. Cone photoreceptor classification in the living human eye from photostimulation-induced phase dynamics. *Proc Natl Acad Sci USA*. 2019;116:7951–7956.
13. Hillmann D, Spahr H, Pfäffle C, Sudkamp H, Franke G, Hüttmann G. In vivo optical imaging of physiological responses to photostimulation in human photoreceptors. *Proc Natl Acad Sci USA*. 2016;113:13138–13143.
14. Cooper RF, Brainard DH, Morgan JI. Optoretinography of individual human cone photoreceptors. *Opt Express*. 2020;28:39326–39339.
15. Azimipour M, Valente D, Vienola KV, Werner JS, Zawadzki RJ, Jonnal RS. Optoretinogram: optical measurement of human cone and rod photoreceptor responses to light. *Opt Lett*. 2020;45:4658–4661.
16. Pandiyan VP, Nguyen PT, Pugh EN, Jr, Sabesan R. Human cone elongation responses can be explained by photoactivated cone opsin and membrane swelling and osmotic response to phosphate produced by RGS9-catalyzed GTPase. *Proc Natl Acad Sci USA*. 2022;119:e2202485119.
17. Lassoued A, Zhang F, Kurokawa K, et al. Cone photoreceptor dysfunction in retinitis pigmentosa revealed by optoretinography. *Proc Natl Acad Sci USA*. 2021;118:e2107444118.
18. Gaffney M, Connor TB, Cooper RF. Intensity-based optoretinography reveals sub-clinical deficits in cone function in retinitis pigmentosa. *Front Ophthalmol*. 2024;4:1373549.
19. Hood DC, Lazow MA, Locke KG, Greenstein VC, Birch DG. The transition zone between healthy and diseased retina in patients with retinitis pigmentosa. *Invest Ophthalmol Vis Sci*. 2011;52:101–108.
20. Chen M, Cooper RF, Han GK, Gee J, Brainard DH, Morgan JI. Multi-modal automatic montaging of adaptive optics retinal images. *Biomed Opt Express*. 2016;7:4899–4918.
21. Scoles D, Sulai YN, Langlo CS, et al. In vivo imaging of human cone photoreceptor inner segments. *Invest Ophthalmol Vis Sci*. 2014;55:4244–4251.
22. Watson AB, Pelli DG. QUEST: a Bayesian adaptive psychometric method. *Percept Psychophys*. 1983;33:113–120.
23. Rodieck R. The density recovery profile: a method for the analysis of points in the plane applicable to retinal studies. *Vis Neurosci*. 1991;6:95–111.
24. Roorda A, Metha AB, Lennie P, Williams DR. Packing arrangement of the three cone classes in primate retina. *Vis Res*. 2001;41:1291–1306.
25. Wang Q, Tuten WS, Lujan BJ, et al. Adaptive optics microperimetry and OCT images show preserved function and recovery of cone visibility in macular telangiectasia type 2 retinal lesions. *Invest Ophthalmol Vis Sci*. 2015;56:778–786.
26. Hood DC, Lin CE, Lazow MA, Locke KG, Zhang X, Birch DG. Thickness of receptor and post-receptor retinal layers in patients with retinitis pigmentosa measured with frequency-domain optical coherence tomography. *Invest Ophthalmol Vis Sci*. 2009;50:2328–2336.
27. Curcio CA, Allen KA, Sloan KR, et al. Distribution and morphology of human cone photoreceptors stained with anti-blue opsin. *J Comp Neurol*. 1991;312:610–624.
28. Sayo A, Ueno S, Kominami T, et al. Significant relationship of visual field sensitivity in central 10 to thickness of retinal layers in retinitis pigmentosa. *Invest Ophthalmol Vis Sci*. 2018;59:3469–3475.
29. Rangaswamy NV, Patel HM, Locke KG, Hood DC, Birch DG. A comparison of visual field sensitivity to photoreceptor thickness in retinitis pigmentosa. *Invest Ophthalmol Vis Sci*. 2010;51:4213–4219.
30. Foote KG, De la Huerta I, Gustafson K, et al. Cone spacing correlates with retinal thickness and microperimetry in patients with inherited retinal degenerations. *Invest Ophthalmol Vis Sci*. 2019;60:1234–1243.
31. Dunn FA, Lankheet MJ, Rieke F. Light adaptation in cone vision involves switching between receptor and post-receptor sites. *Nature*. 2007;449:603–606.
32. Lee JY, Care RA, Kastner DB, Della Santina L, Dunn FA. Inhibition, but not excitation, recovers from partial cone loss with greater spatiotemporal integration, synapse density, and frequency. *Cell Rep*. 2022;38:110317.
33. Ellis EM, Paniagua AE, Scalabrino ML, et al. Cones and cone pathways remain functional in advanced retinal degeneration. *Curr Biol*. 2023;33:1513–1522.e1514.
34. Telias M, Denlinger B, Helft Z, Thornton C, Beckwith-Cohen B, Kramer RH. Retinoic acid induces hyperactivity, and blocking its receptor unmasks light responses and augments vision in retinal degeneration. *Neuron*. 2019;102:574–586.e575.
35. Iga Y, Hasegawa T, Ikeda HO, et al. Progression of retinitis pigmentosa on static perimetry, optical coherence tomography, and fundus autofluorescence. *Sci Rep*. 2023;13:22040.
36. Jiang X, Liu T, Pandiyan VP, Slezak E, Sabesan R. Coarse-scale optoretinography (CoORG) with extended field-of-view for normative characterization. *Biomed Opt Express*. 2022;13:5989–6002.
37. Zhang P, Zawadzki RJ, Goswami M, et al. In vivo optophysiology reveals that G-protein activation triggers osmotic swelling and increased light scattering of rod photoreceptors. *Proc Natl Acad Sci USA*. 2017;114:E2937–E2946.

Investigative Ophthalmology & Visual Science

38. Ji Q, Liu Y, Bernucci MT, Crowell JA, Miller DT. Method for assessing structure and function of cone photoreceptors with multiple outer segment reflections in healthy and diseased eyes. In: *Ophthalmic Technologies XXXIV*. *SPIE*; 2024:41–47, https://doi.org/10.1117/12.3003241.
39. Birch DG, Sandberg MA, Berson EL. The Stiles-Crawford effect in retinitis pigmentosa. *Invest Ophthalmol Vis Sci*. 1982;22:157–164.
40. Yusuf IH, Birtel J, Shanks ME, et al. Clinical characterization of retinitis pigmentosa associated with variants in SNRNP200. *JAMA Ophthalmol*. 2019;137:1295–1300.
41. Chen X, Liu Y, Sheng X, et al. PRPF4 mutations cause autosomal dominant retinitis pigmentosa. *Hum Mol Genet*. 2014;23:2926–2939.
42. Pandiyan VP, Jiang X, Kuchenbecker JA, Sabesan R. Reflective mirror-based line-scan adaptive optics OCT for imaging retinal structure and function. *Biomed Opt Express*. 2021;12(9):5865–5880.
43. Pandiyan VP, Jiang X, Maloney-Bertelli A, Kuchenbecker JA, Sharma U, Sabesan R. High-speed adaptive optics line-scan OCT for cellular-resolution optoretinography. *Biomed Opt Express*. 2020;11(9):5274–5296.